Measuring Effective Diffusivity in Porous Media with a Gasket-Free, Radial Arrangement

Yongwook Kim, Jeff T. Gostick*

Department of Chemical Engineering, University of Waterloo, Waterloo, ON Canada

*Corresponding Author: jgostick@uwaterloo.ca

Keywords

Effective diffusion coefficient; Tortuosity; Bruggeman; Porous media

Abstract

A simple technique for measuring the effective diffusivity, and ultimately tortuosity, in porous media is presented. The method uses a custom-built apparatus, based on a radial geometry, which eliminates the need for any gaskets to seal the edge of the sample. This makes it particularly well suited for thin media such as films and layers. The experiment is based on the transient response of the oxygen concentration at the center of the sample as oxygen diffuses into an initially nitrogen filled domain from the sample perimeter. The analytical solution of Fick's law for transient diffusion in cylindrical coordinates is fitted to the measured oxygen concentration profile to obtain the effective diffusivity. To validate the method, binary diffusion coefficients of N_2-Air system were measured and the results show a close match and are consistent for a range of experimental parameters like flow rate and domain thickness. The classical study of diffusion in porous media based on sphere packing is revisited for further validation of the technique. The results show good agreement to the well-known Bruggeman correlation as well as to the experimental values reported in the literature. The new technique is further applied to other types of thin porous materials and the results indicate that the Bruggeman correlation generally underestimates the effective diffusivity of non-sphere packing.

1. Introduction

The effective diffusivity in thin porous media is of great importance in modern engineering applications. Energy conversion and storage devices such as fuel cells [1–4] and metal-air batteries [5] as well as water desalination [6,7], filtration and separation [8], and gas sensors [9,10] are just a few examples. In many of these applications, the performance of the device is highly dependent on the diffusive transport; therefore, accurate ex-situ characterization is crucial to producing high performing engineered porous media. Unfortunately, there isn't yet a well-established, easy to apply and standardized method for characterizing the effective diffusivity in thin porous media due to the geometrical constraints imposed by their thinness.

Despite the challenge, there has been numerous attempts to develop a technique for measuring the effective diffusivity in thin porous media. The Loschmidt apparatus is a classic technique [11] for measuring binary diffusion coefficient where two gases of interest are filled in two separate compartments. The compartments are initially separated by closing the connection, then the connection is opened to allow gases to diffuse into one another. The transient gas concentrations are measured as a function of time to obtain the binary diffusion coefficient. Astrath *et al.* [12] modified the original Loschmidt cell by measuring the gas concentration as a function of time at a fixed position, thereby measuring the diffusivity transiently. Zamel *et al.* [13] adopted this method and modified it even further to study the effective diffusion in gas diffusion layers (GDL) in proton exchange membrane fuel cells (PEMFC). In their work, two gas compartments were separated by a GDL, which has a thickness range from 200 – 400 μm, effectively adding resistance to the bulk diffusion. The delay induced by the porous sample can be used to extract the effective diffusivity. This technique was subsequently used to characterize the effective diffusivity in the catalyst layer in PEMFC, though with considerably more complexity [14]. A significant limitation of the modified Loschmidt cell generally is that it requires the sample to be self-standing which might not be possible in some cases. Also, it is questionable whether such thin materials will add

noticeable resistance to the bulk diffusion process. Another classical measurement technique is the Wicke-Kallenbach (W-K) diffusion cell [15]. In the W-K type cells, a porous sample is placed between two gas flow channels where two different types of gases flow in each channel. The concentration gradient across the porous sample drives the gas diffusion into the porous sample. Secanell and co-workers [16–18] adopted the W-K cell and used it to measure the effective diffusivity in GDLs. The modified W-K cell was also used by workers at General Motors to measure the effective diffusivity in the catalyst layer (CL) of PEMFC [19]. The main drawbacks of the W-K type technique are that careful control of the gas flow rate and extremely accurate measurement of the gas concentration is required since the effective diffusivity is extracted based on the mass balance around the diffusion cell. Because materials such as GDLs and CLs are so thin, even a slight pressure difference can cause significant convective flow. An alternative approach to measuring diffusivity was used by Rashapov *et al.* [20]. They developed a simple technique based on the transient diffusion of oxygen into a porous sample initially filled with nitrogen. The concentration of oxygen is measured at a fixed position as a function of time and the analytical solution of the Fick's second law is fitted to the experimental data to extract the effective diffusivity. This technique was subsequently applied to dry [21] and partially saturated [22] GDLs. Although quite convenient, this technique required application of sealing material on the edges to prevent diffusion and satisfy the boundary condition of the analytical solution of 1-D diffusion in a planar sheet. This can be problematic for thinner materials such as CL. Perhaps the most well-established method for measuring effective diffusivity in porous media is to flood the pore space with liquid brine and measure the ionic conductivity. The analogy between Ohm's law and Fick's law is used to indirectly obtain formation factor. This is generally not applicable in many porous media of interest as they are often made with conductive materials, which complicates the interpretation and implementation of these experiments considerably [23,24]. It is also quite difficult to ensure that materials are fully saturated with brine, especially if they've been given a hydrophobic treatment of some sort [25].

In this work, a novel and simple technique for measuring the effective diffusivity in thin porous media is developed. This method is a variation to the earlier work done by Rashapov *et al.* [20], but adopting a radial geometry instead, which has several advantages: 1) no sealing is required, therefore it is easily applicable even to ultrathin materials, 2) because no seal is required there is no need to apply pressure to the sample holder which might damage or deform the sample, and 3) the measurement time is only on the order of minutes. The newly developed method was thoroughly validated and applied to classical porous media such as sphere packing.

2. Experimental Methods

The radial diffusivity apparatus consists of two specially designed sample mounts or pedestals (top and bottom), a cylindrical chamber for gas flow and a fiber optic O_2 sensor. All components of the apparatus were built in-house except for the optical oxygen sensor which was purchased from Pyro-Science (Aachen, Germany). The O_2 sensor used in this study was ultra-fast response sensor (OXR430-UHS) with the response time less than 0.3 seconds according to the manufacturer and verified in the lab.

2.1. Diffusion Pedestals

The top and bottom pedestals were designed and machined as shown in Figure 1(left). The O_2 sensor probe (a fiber optic strand of 0.43 mm diameter) was positioned through the center of the top pedestal and the tip of the sensor was aligned with the surface of the top pedestal. A hole for the sensor was drilled in two stages where a smaller hole that matched the sensor diameter was first made and subsequently a larger hole that was filled with silicone elastomer to seal around the fiber. Two levels of holes were necessary as friction fit of the sensor with just a single hole resulted in a significant amount leakage into the sample due to gaps between the hole itself and the sensor, which led to error in the measurement. The base of the sample mounts was designed with a sliding fit inside the cylindrical chamber to guide and position them, while the pedestal portion was slightly smaller. This created a small gap around the perimeter of the sample stage for N_2 gas to flow by the sample perimeter with high velocity. The neck of the pedestal was designed with an angle so that the gas is smoothly supplied to the sample perimeter.

2.2. System Setup and Test Procedure

The entire system setup in shown in Figure 1(right). A porous sample of 1.25-inch in diameter was placed on the sample stage of the bottom pedestal and they were placed inside the cylindrical chamber. The top pedestal was then slid into the chamber and

gently onto of the sample. N_2 gas was supplied from the bottom and distributed to the system through the holes on the pedestal and exited through the top.

Prior to each experiment, the oxygen sensor was calibrated according to the local environmental conditions (i.e. temperature, pressure, humidity) to ensure O_2 reading of 20.9%. Temperature and pressure were measured externally, and humidity was measured internally by the O_2 sensor electronics. The porous sample was placed on the bottom pedestal and left under the ambient condition for at least half an hour to establish initial oxygen concentration of 20.9% everywhere within the porous domain.

The data logging is initiated at $t = 0$ and approximately after 5 seconds, N_2 supply was turned on to allow the flow N_2 gas past the sample perimeter. N_2 gas was supplied at high flow rate to ensure nearly instantaneous change in the boundary condition. The depletion of the oxygen concentration at the center of the sample was measured and recorded as a function of time. After a constant value of 0% oxygen was recorded for at least 20 seconds, data logging was stopped.

2.3. Data Analysis

The effective diffusion coefficient was extracted by fitting the analytical solution of the Fick's second law for cylindrical coordinates to the oxygen concentration profile obtained experimentally. Assuming diffusion is everywhere radial within the sample, the Fick's law of transient diffusion is written as:

$$\frac{\partial C_i}{\partial t} = \frac{1}{r}\frac{\partial}{\partial r}\left(rD\frac{\partial C_i}{\partial r}\right) \quad \textbf{[1]}$$

where C_i is the concentration of species i, r is the spatial coordinate along the concentration gradient, t is time and D is the diffusion coefficient. Eq. [1] can be solved analytically with the following boundary conditions:

$$C(t) = \begin{cases} C_0, & r = R, \quad t \geq 0 \\ C_1, & 0 < r < R, \quad t = 0 \end{cases} \quad \textbf{[2]}$$

where $C(t)$ is the concentration as a function of time at a fixed position r, R is the radius of the sample, C_0 is the constant surface concentration and C_1 is the initial

concentration distribution of the species within the sample. The analytical solution for such case is provided by Crank [26]:

$$\frac{C(t) - C_1}{C_0 - C_1} = 1 - \frac{2}{R}\sum_{n=1}^{\infty} \frac{\exp(-D\alpha_n^2 t)\, J_0(\alpha_n r)}{\alpha_n J_1(\alpha_n R)} \quad \textbf{[3]}$$

where $J_0(r)$ and $J_1(r)$ are the Bessel functions of the first kind of order 0 and 1, respectively. α_n is defined in Eq. [4] where $\alpha_n R$ are the n^{th} root of:

$$J_0(\alpha_n R) = 0 \quad \textbf{[4]}$$

After obtaining the oxygen concentration profile, $C(t)$, the only unknown variable in Eq. [3] is the diffusion coefficient, D. Therefore, Eq. [3] can be fitted to the experimental data by the method of least squares.

Figure 2 shows an example of the above analytical solution fitted to the experimental data for N_2 diffusion in open air. As evident from Figure 2, the analytical solution fits well to the experimental data. It is also noteworthy that for open air the steady-state is expected to be reached within 15 seconds. The rapid experimental time can be beneficial especially for samples with lower porosity or smaller pore sizes where the diffusion takes place at a much slower rate, but it does necessitate the use of a high response time oxygen probe.

It should also be pointed out that the effective diffusivity obtained from the above procedure is not in the same sense as the one most widely used:

$$D_{eff} = (\varepsilon/\tau) D_b \quad \textbf{[5]}$$

where D_{eff} is the effective diffusivity in porous media, D_b is the bulk diffusivity of a binary system, ε is the porosity and τ is the tortuosity of the porous sample.

This can be explained by performing a transient mass balance around the porous media. Assuming incompressible fluid flow with no convection and no reaction, the continuity equation in porous media can be expressed as [27]:

$$\varepsilon \frac{\partial C}{\partial t} = D_{eff} \nabla^2 C \quad \textbf{[6]}$$

In Eq. [6], ε is multiplied to the transient term (LHS) since, in porous media, the volume where gas species can reside is decreased by a factor of ε. In other words, C is defined as $\mathrm{mol/m^3}$ of sample, but the gas molecules are confined to the pore space so the oxygen concentration measurement is $\mathrm{mol/m^3}$ of void space, thus the measured concentration must be multiplied by ε for application in Eq. [6]. On the RHS, the flux is also decreased by the presence of solid phase which is already embedded in the definition of the effective diffusivity given by Eq. [5]. Therefore, substituting Eq. [5] into Eq. [6] effectively cancels out ε on both sides, resulting in:

$$\frac{\partial C}{\partial t} = \left(\frac{D_b}{\tau}\right) \cdot \nabla^2 C \qquad \textbf{[7]}$$

This means that the *effective diffusivity* obtained from the current technique should be interpreted as $(1/\tau)D_b$, not as $(\varepsilon/\tau)D_b$. This is actually one of the interesting aspects of the current method where tortuosity, τ, is measured directly, independent of the porosity.

2.4. Sample Preparation

Three types of porous medium were considered for testing: 1) monodispersed random sphere packing, 2) polydispersed agglomerated sphere packing and 3) quartz frits with non-ideal pore shape. Tested samples are summarized in Table 1. SEM Images of each sample are shown in Figure 3.

Due to the nature of sphere particles not being able to form a rigid structure, a special method for preparing porous disc was adopted. For glass, silica and alumina materials, they were first dispersed in water. Then, the dispersion was filtered through a membrane with the average pore size of 0.03 μm. The dispersion was stirred as they were being poured into the filtration apparatus to achieve a “random” packing of sphere particles. The filtered deposits on the membrane were cut into 1.25-inch diameter disc and placed onto the bottom pedestal. The membrane was carefully peeled off and the sample was dried at 80°C until constant mass was measured.

For stainless steel (440C type) balls, a sheet of flexible magnet was purchased.

Flexible magnet was cut into 1.25-in diameter disc and was attached to the sample stage of the bottom pedestal. The stainless steel balls were then poured onto the flexible magnet in a packing die made in-house and gently packed, just enough to make the top surface flat.

30 mm disc of quartz frits of various porosities (Table 1) were purchased from Technical Glass Products and tested as-received since they were already made into a disc shape.

2.5. Porosity Measurement

The effective diffusivity is generally a decreasing function of porosity, therefore porosities of each sample tested were measured. The method of measuring porosity was also altered according to the nature of the sample. For monodispersed spheres (glass, stainless steel and silica) and polydispersed agglomerated spherical particles (alumina), "tapped density" was measured and it was used to calculate porosity. Particles were measured to a certain weight and they were placed in a 10-mL graduated cylinder. The graduated cylinder was repeatedly tapped until there was no more volume change. Tapped density of the particles was calculated using Eq. [8].

$$\rho_{tapped} = \frac{m_s}{V_{tapped}} \quad \textbf{[8]}$$

where ρ_{tapped} is the tapped density of the particles, m_s is the mass of the solid and V_{tapped} is the final tapped volume. This process mimicked the sample preparation process as filtration of randomly dispersed particles will result in "a tight random" packing of the particles. The porosity of the sample was calculated using the following equation:

$$\varepsilon = 1 - \frac{\rho_{tapped}}{\rho_s} \quad \textbf{[9]}$$

where ε is the porosity of the sample from (0 – 1) and ρ_s is the density of the pure solid. Since, bulk densities of the solids tested are well known, the porosities can also be calculated.

Porosities of quartz frits were measured using the buoyancy technique [28]. Thickness of the quartz frits were measured with a micrometer with 1 µm resolution and $\pm$0.1 µm accuracy. The sample was then weighed both dry and submerged in highly wetting silicone oil (5 cSt). Implementing Archimedes' principle allowed the determination of the pure solid density and ultimately the porosity of the sample.

2.6. Validation with Open Air

Validity of the radial diffusivity apparatus was analyzed by measuring bulk diffusivity of nitrogen-air (N_2-Air) binary system with no sample present between the pedestals, only an empty gap. To ensure that the diffusion was the only mode of mass transport during the experiment, bulk diffusivity measurement was performed with different gap distances between the pedestals and with different N_2 gas flow rates.

The results for binary diffusion coefficients of N_2-Air system with various gap distance is shown in Figure 4(left). In Figure 4(left), the red line indicates the theoretical bulk diffusion coefficient of N_2-Air system estimated by the Chapman-Enskog equation [29]:

$$D_{ij} = \frac{0.00186 \cdot T^{3/2}}{P \cdot \sigma_{ij}^2 \cdot \Omega} \left(\frac{1}{M_i} + \frac{1}{M_j} \right)^2 \quad \textbf{[10]}$$

where D_{ij} is the binary diffusion coefficient of species i and j measured in cm^2/s, T is the temperature in Kelvin, P is the pressure in atmospheres, and M_i and M_j are the molecular weights of species i and j, respectively. σ_{ij} and Ω are Lennard-Jones potential parameters from the Chapman-Enskog theory where the values for various species are given elsewhere [29].

The average of binary diffusion coefficients measured at different gap distances with the value of 0.203 cm^2/s and the deviation of 1.03%. Figure 4(right) shows the binary diffusion coefficients of N_2-Air system tested with various volumetric flow rates of N_2 gas. Again, in Figure 4(right), the red line shows the binary diffusion coefficient of N_2-Air estimated by the Chapman-Enskog theory. The average value was 0.202 cm^2/s with the

deviation of 3.31%. The results indicate that the binary diffusion coefficient depends neither on the gap distance nor on the volumetric flow rates and confirms that the diffusion is the only mode of the mass transport in the experiments.

One of the challenges in designing a diffusivity experiment is keeping the boundary condition constant as oxygen diffusing out of the sample can result in the change in boundary condition. This problem was resolved by using the flow rate of 1500 sccm for N_2 gas. From Figure 2, for open air, the steady state is reached approximately 10 seconds after the boundary condition has been applied ($C_{O_2} = 0$). At the flow rate of 1500 sccm N_2, the total number of moles of N_2 entering the sample perimeter is 1.022×10^{-2} mol N_2. Assuming the bottom and the top pedestals are approximately 2 mm apart, there would be 1.35×10^{-5} mol O_2 and 5.12×10^{-5} mol N_2 within the open space initially. After approximately 10 seconds, all O_2 molecules would have diffused out of the open space and the balancing moles of N_2 would have diffused into the open space from the gas flow. Then, the gas flow leaving the top of the gap would have O_2 concentration of approximately 0.1% and N_2 concentration of 99.9%. The concentration change within the gas flow is minimal, therefore it is valid to assume the boundary conditions are constant throughout the experiment. This is also illustrated in Figure 5. The concentration change will be even lower for the thin engineered porous media since their thicknesses are generally within micrometer range. Also, the diffusion process is slower for the porous materials than it is for the bulk diffusion in the open space. High flow rate will not only change the boundary condition instantly, but also will flush away the trace amount of oxygen diffusing out of the sample immediately, effectively keeping the boundary condition constant

3. Results and Discussion

The radial diffusivity apparatus was tested with various porous media with different pore geometries (i.e. shape and size). Spherical particles were extensively tested since sphere packings are the most well studied porous media experimentally and theoretically. Agglomerated spherical alumina packing and quartz frits were chosen to investigate the ability of the apparatus to measure porous media with other types of pore geometry.

Figure 6 shows the relative diffusivity (D_{eff}/D_b) of the sphere packing with various sizes and materials. The experimental values were compared to the Bruggeman [30] and Neale and Nader [31] approximations. There are many published models for estimating the tortuosity factor of porous media, however, the Bruggeman and Neale and Nader were chosen because two correlations were specifically developed for random homogeneous isotropic sphere packing.

Although, the Bruggeman approximation is most commonly used to estimate the effective diffusivity, there are numerous reports where the model overestimates the effective diffusivity, especially for low porosity [1,19,32,33]. What is often overlooked is that the original equation derived by the Bruggeman is actually $D_{eff}/D_b = \varepsilon^{(1+n)/n}$, or simply $D_{eff}/D_b = \varepsilon^m$, where m (or n) is the shape factor. The most widely used form of the Bruggeman equation ($D_{eff}/D_b = \varepsilon^{1.5}$) is a special instance of the Bruggeman's original derivation where the particle shape is spherical (m = 1.5) [30,33]. It is evident from the previous works [34–36], as well as the present work, when assumptions of the approximation are satisfied (random, isotropic spheres), the tortuosity estimated by the Bruggeman agrees well with the experimental measurements. In many cases of interest to engineers, however, the shape of the particles is much more complex than spheres, hence the Bruggeman equation must be used with caution. Gaseous diffusion in glass sphere packing of various particle sizes was experimentally investigated by Currie [35]. Comparison between the values obtained by Currie and the present study is illustrated in Figure 7. The values lie in the higher porosity region are stainless steel sphere packing.

For glass sphere packing, Currie and the present study showed similar porosity as well as the relative diffusivity. Generally, the tortuosity in both studies either followed the Bruggeman correlation or were just slightly underestimated by it.

The tortuosity of the quartz frits had higher values than what the Bruggeman correlation predicted (Figure 6). This problem is commonly encountered when the particle shape of the porous media deviates from the ideal spherical shape. This was also seen from Currie's work where higher Bruggeman exponents were obtained for most porous media. Currie attempted to calculate the relative surface area (S_γ) of the tested materials where S_γ was defined as the ratio of the surface area of the material to that of a sphere with equal volume. Although, no mathematical description was given, the experimental data showed a general trend where with increasing relative surface area, the shape factor increased [35]. Some works claim that the deviation is attributed the anisotropy of the porous structure [37], however it is still unclear as to why such behavior is observed. An attempt was made to obtain the Bruggeman exponent that fits the quartz frits data by least-square method, and m = 1.75 was obtained.

Packing of the agglomerated spherical alumina particles exhibited effective diffusion behavior well below the Bruggeman correlation. The effect is even more dramatic than that of the quartz frits because Knudsen diffusion is expected to play a significant role due to small pore sizes of the alumina packings. From Figure 6, it can be seen that the relative diffusivity of alumina packing with particle size 0.3 – 0.8 µm deviates even more from the Bruggeman than the alumina packing with particle size 3.5 – 15 µm does since alumina packing with 0.3 – 0.8 µm particles are expected to have smaller pore size, hence a stronger Knudsen effect was expected. Pore size distributions of each Al_2O_3 particle size were roughly estimated from the SEM images and the result is shown in Figure 8. As expected, the pore size distribution of 0.3 – 0.8 µm alumina packing falls in the lower region with the average pore diameter of approximately 31 nm. 3.5 – 15 µm alumina packing had larger and broader pore size distribution with the average pore diameter of around 103 nm. Fitting the Bruggeman equation here is nonsensical since the diffusion in alumina packing is not only affected by the pore size. In Bruggeman's

equation, pore size effect was never considered therefore should not be used outside of the molecular diffusion regime. Nonetheless the experimental data obtained by the present experiment are self-consistent and suggest that the tool can be used for effective diffusivity determination in such nanoporous media, though a more complex data analysis is beyond the scope of this work.

4. Conclusion

A simple and effective experimental technique for measuring the effective diffusivity of thin porous materials has been developed. The apparatus adopted a non-steady state approach of measuring the diffusivity with a radial geometry. Samples were initially filled with air, and oxygen was allowed to diffuse out of the sample by supplying high flow rate of N_2 gas along the perimeter of the sample. The transient oxygen concentration profile obtained from the radial diffusivity apparatus was fitted to the analytical solution of the Fick's law of transient diffusion in cylindrical coordinates to obtain the effective diffusivity. The method was validated by measuring the binary diffusion coefficient of N_2-Air system with various gap distances and flow rates and it was shown that the gap distances and the flow rates had no effect on the measured binary bulk diffusivity.

The radial diffusivity apparatus was applied to the classical sphere packing as well as other types of porous media such as agglomerated alumina packing and quartz frits. Diffusivity in sphere packing showed good agreement with the well-known Bruggeman correlation whereas the other types of porous media exhibited lower values than predicted by the Bruggeman correlation. The method is therefore sensitive enough to detect Knudsen effects, though a full analysis of this behavior was beyond the scope of this work.

Besides the fact that the current method is exceedingly simple to implement, the other crucial advantage of the radial diffusivity apparatus is that it requires no sealing, therefore can be easily applied even to ultrathin porous layers. With the recent interest in porous electrode used in energy applications such as batteries and fuel cells, the radial diffusivity apparatus can be quite powerful as most electrodes are made extremely thin to minimize the mass and charge transport limitations. Gas sensing devices are another potential application where a thin porous layer is used to detect various hazardous gases and vapors.

As with most techniques, the radial diffusivity apparatus has certain limitations. The technique is only able to measure the effective diffusivity in the in-plane direction, thus

if the material possesses an anisotropic structure with different in-plane and through-plane properties, such as fibrous media, only the in-plane component of the effective diffusivity tensor can be obtained. In cases where the in-plane properties vary between the x and y directions, as in fibrous media with aligned fibers, the proposed method would be very difficult to interpret and essentially invalid.

Acknowledgement

This work was financially supported by the Natural Science and Engineering Research Council (NSERC) of Canada and the Automotive Fuel Cell Corporation (AFCC).

References

[1] J.G. Pharoah, K. Karan, W. Sun, On effective transport coefficients in PEM fuel cell electrodes: Anisotropy of the porous transport layers, J. Power Sources. 161 (2006) 214–224.

[2] L. Zhang, H.T. Bi, D.P. Wilkinson, J. Stumper, H. Wang, Gas-liquid two-phase flow patterns in parallel channels for fuel cells, J. Power Sources. 183 (2008) 643–650.

[3] R. Anderson, L. Zhang, Y. Ding, M. Blanco, X. Bi, D.P. Wilkinson, A critical review of two-phase flow in gas flow channels of proton exchange membrane fuel cells, J. Power Sources. 195 (2010) 4531–4553.

[4] H. Zarrin, D. Higgins, Y. Jun, Z. Chen, M. Fowler, Functionalized graphene oxide nanocomposite membrane for low humidity and high temperature proton exchange membrane fuel cells, J. Phys. Chem. C. 115 (2011) 20774–20781.

[5] F. Cheng, J. Chen, Metal-air batteries: From oxygen reduction electrochemistry to cathode catalysts, Chem. Soc. Rev. 41 (2012) 2172–2192.

[6] K.C. Smith, Theoretical evaluation of electrochemical cell architectures using cation intercalation electrodes for desalination, Electrochim. Acta. 230 (2017) 333–341.

[7] S. Liu, K.C. Smith, Quantifying the Trade-offs between Energy Consumption and Salt Removal Rate in Membrane-free Cation Intercalation Desalination, Electrochim. Acta. 271 (2018) 652–665.

[8] W.J. Koros, R. Mahajan, Pushing the limits on possibilities for large scale gas separation: which strategies?, J. Memb. Sci. 181 (2001) 141.

[9] A. Cabot, J. Arbiol, A. Cornet, J.R. Morante, F. Chen, M. Liu, Mesoporous catalytic filters for semiconductor gas sensors, Thin Solid Films. 436 (2003) 64–69.

[10] G. Sakai, N. Matsunaga, K. Shimanoe, N. Yamazoe, Theory of gas-diffusion controlled sensitivity for thin film semiconductor gas sensor, Sensors Actuators, B Chem. 80 (2001) 125–131.

[11] A.M. Anderson, Experimental methods for engineers, 1994.

[12] N.G.C. Astrath, J. Shen, D. Song, J.H. Rohling, F.B.G. Astrath, J. Zhou, T. Navessin, Z.S.S. Liu, C.E. Gu, X. Zhao, The effect of relative humidity on binary gas diffusion., J. Phys. Chem. B. 113 (2009) 8369–8374.

[13] N. Zamel, N.G.C. Astrath, X. Li, J. Shen, J. Zhou, F.B.G. Astrath, H. Wang, Z.S. Liu, Experimental measurements of effective diffusion coefficient of oxygen-nitrogen mixture in PEM fuel cell diffusion media, Chem. Eng. Sci. 65 (2010) 931–937.

[14] J. Zhao, S. Shahgaldi, I. Alaefour, Q. Xu, X. Li, Gas permeability of catalyzed electrodes in polymer electrolyte membrane fuel cells, Appl. Energy. 209 (2018) 203–210.

[15] E. Wicke, R. Kallenbach, Die Oberflächendiffusion von Kohlendioxyd in aktiven Kohlen, Kolloid-Zeitschrift. 97 (1941) 135–151.

[16] L.M. Pant, S.K. Mitra, M. Secanell, Absolute permeability and Knudsen diffusivity measurements in PEMFC gas diffusion layers and micro porous layers, J. Power Sources. 206 (2012) 153–160.

[17] N.B. Carrigy, L.M. Pant, S. Mitra, M. Secanell, Knudsen Diffusivity and Permeability of PEMFC Microporous Coated Gas Diffusion Layers for Different Polytetrafluoroethylene Loadings, J. Electrochem. Soc. 160 (2013) F81–F89.

[18] P. Mangal, L.M. Pant, N. Carrigy, M. Dumontier, V. Zingan, S. Mitra, M. Secanell, Experimental study of mass transport in PEMFCs: Through plane permeability and molecular diffusivity in GDLs, Electrochim. Acta. 167 (2015) 160–171.

[19] Z. Yu, R.N. Carter, Measurement of effective oxygen diffusivity in electrodes for proton exchange membrane fuel cells, J. Power Sources. 195 (2010) 1079–1084.

[20] R. Rashapov, F. Imami, J.T. Gostick, A method for measuring in-plane effective diffusivity in thin porous media, Int. J. Heat Mass Transf. 85 (2015) 367–374.

[21] R.R. Rashapov, J.T. Gostick, In-Plane Effective Diffusivity in PEMFC Gas Diffusion Layers, Transp. Porous Media. 115 (2016) 411–433.

[22] T.G. Tranter, P. Stogornyuk, J.T. Gostick, A.D. Burns, W.F. Gale, A method for measuring relative in-plane diffusivity of thin and partially saturated porous media: An application to fuel cell gas diffusion layers, Int. J. Heat Mass Transf. 110

(2017) 132–141.

[23] D. Kramer, S.A. Freunberger, R. Flückiger, I.A. Schneider, A. Wokaun, F.N. Büchi, G.G. Scherer, Electrochemical diffusimetry of fuel cell gas diffusion layers, J. Electroanal. Chem. 612 (2008) 63–77.

[24] R. Flückiger, S.A. Freunberger, D. Kramer, A. Wokaun, G.G. Scherer, F.N. Büchi, Anisotropic, effective diffusivity of porous gas diffusion layer materials for PEFC, Electrochim. Acta. 54 (2008) 551–559.

[25] X. Li, F. Forouzandeh, A.J. Kakanat, F. Feng, D.W.H. Banham, S. Ye, D.Y. Kwok, V. Birss, Surface Characteristics of Microporous and Mesoporous Carbons Functionalized with Pentafluorophenyl Groups, ACS Appl. Mater. Interfaces. 10 (2018) 2130–2142.

[26] J. Crank, The Mathematics of Diffusion, 2nd ed., Oxford University Press, 1975.

[27] L. Shen, Z. Chen, Critical review of the impact of tortuosity on diffusion, Chem. Eng. Sci. 62 (2007) 3748–3755.

[28] R.R. Rashapov, J. Unno, J.T. Gostick, Characterization of PEMFC Gas Diffusion Layer Porosity, J. Electrochem. Soc. 162 (2015) F603–F612.

[29] J.O. Hirschfelder, R.B. Bird, E.L. Spotz, The Transport Properties of Gases and Gaseous Mixtures. II., Chem. Rev. 44 (1949) 205–231.

[30] D.A.G. Bruggeman, Berechnung verschiedener physikalischer Konstanten von heterogenen Substanzen. I. Dielektrizitätskonstanten und Leitfähigkeiten der Mischkörper aus isotropen Substanzen, Ann. Phys. 416 (1935) 636–664.

[31] G.H. Neale, W.K. Nader, Prediction of transport processes within porous media: Diffusive flow processes within an homogeneous swarm of spherical particles, AIChE J. 19 (1973) 112–119.

[32] A.Z. Weber, J. Newman, Modeling transport in polymer-electrolyte fuel cells, 2004.

[33] B. Tjaden, S.J. Cooper, D.J. Brett, D. Kramer, P.R. Shearing, On the origin and application of the Bruggeman correlation for analysing transport phenomena in electrochemical systems, Curr. Opin. Chem. Eng. 12 (2016) 44–51.

[34] J. Hoogschagen, Diffusion in porous catalysts and adsorbents, Ind. Eng. Chem. 47

(1955) 906–912.

[35] J.A. Currie, Gaseous Diffusion in Porous Media .2. Dry Granular Materials, Br. J. Appl. Phys. 11 (1960) 318–324.

[36] M. Ebner, D.W. Chung, R.E. García, V. Wood, Tortuosity anisotropy in lithium-ion battery electrodes, Adv. Energy Mater. 4 (2014) 1–6.

[37] H.L. Penman, Gas and vapour movements in the soil: I. The diffusion of vapours through porous solids, J. Agric. Sci. 30 (1940) 437.

Tables and Figures

Table 1 Summary of Porous Samples Tested for Diffusivity Measurement

Category	Material	Size [μm]	Porosity [-]
Monodispersed Random Sphere	Glass	100	0.39*
		1000	0.40*
	Stainless Steel	3000	0.46*
		2500	0.44*
		1500	0.45*
		1000	0.45*
	Silica	25	0.46*
Polydispersed Agglomerated Sphere	Alumina	3.5 – 15	0.79*
		0.3 – 0.8	0.73*
Quartz Frits	Quartz frits	200 – 300§	0.627**
		40 – 90§	0.452**
		4 – 15§	0.412**

* tapped density
** buoyancy technique[28]
§ given by manufacturer

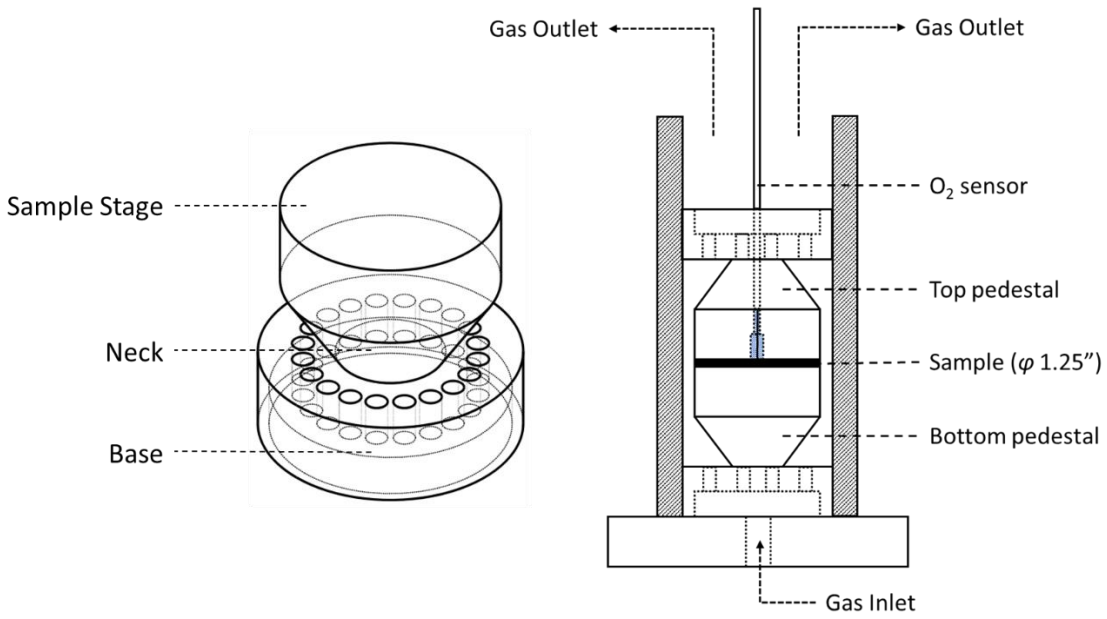

Figure 1 (left) Pedestal design for radial diffusivity apparatus (right) Radial diffusivity apparatus system setup

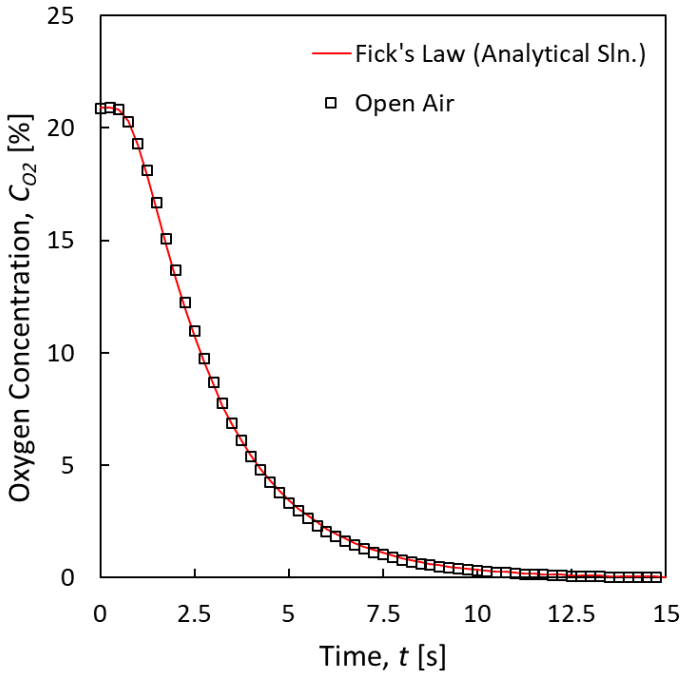

Figure 2 The analytical solution of Fick's second law fitted to transient oxygen concentration profile of an open air

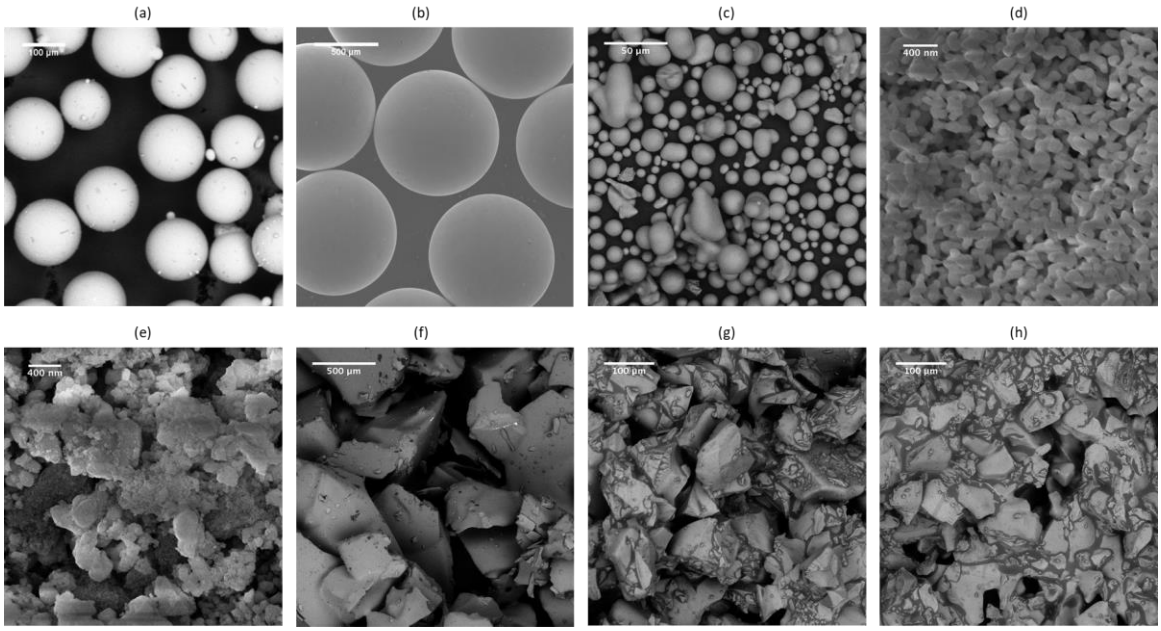

Figure 3 SEM Images of (a) 0.1 mm glass beads, (b) 1 mm stainless steel balls, (c) 25 µm spherical SiO_2, (d) 3.5-15 µm Al_2O_3, (e) 0.3-0.8 µm Al_2O_3, (f) quartz frits with pore size 200 – 300 µm, (g) quartz frits with pore size 40 – 90 µm, (h) quartz frits with pore size 4 – 15 µm

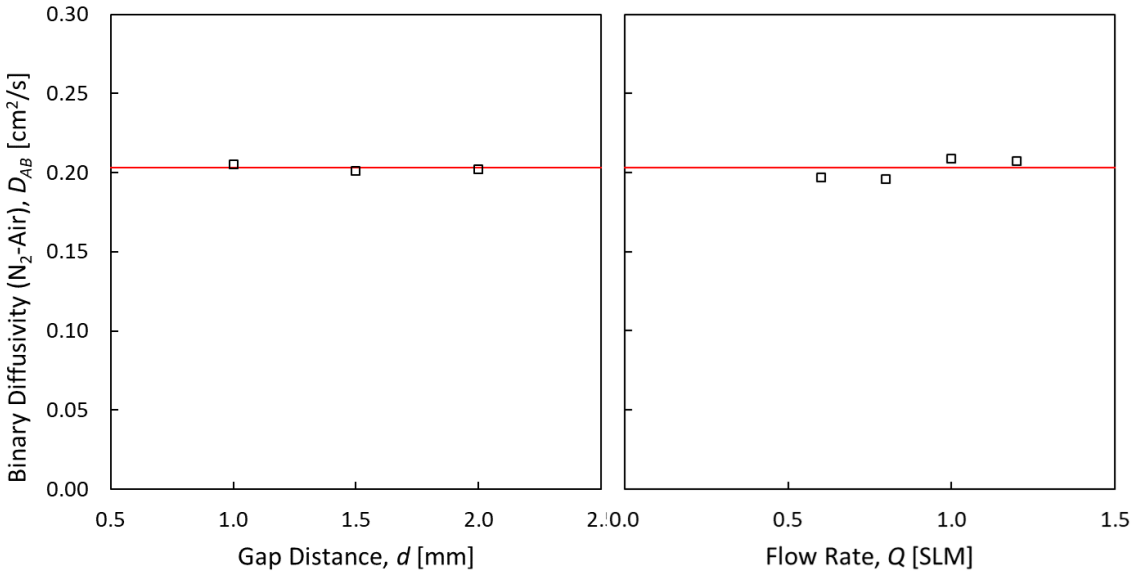

Figure 4 Diffusion coefficient of N_2-Air binary system measured with various gap distances (left) and various volumetric flow rates (right). The line indicates the prediction of the Chapman-Enskog equation given in Eq. **[**10**]**

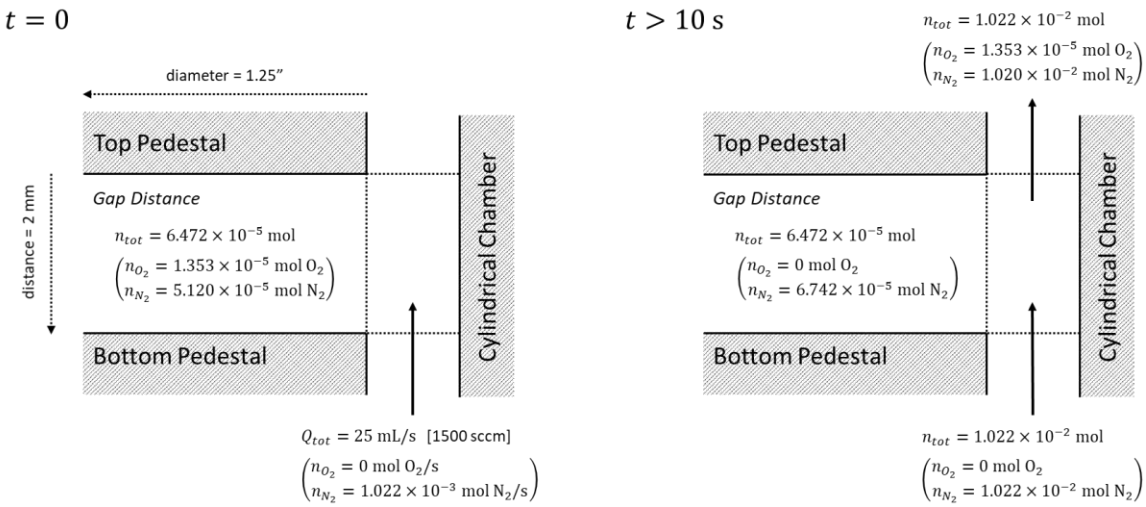

Figure 5 Illustration on justification of the constant boundary condition

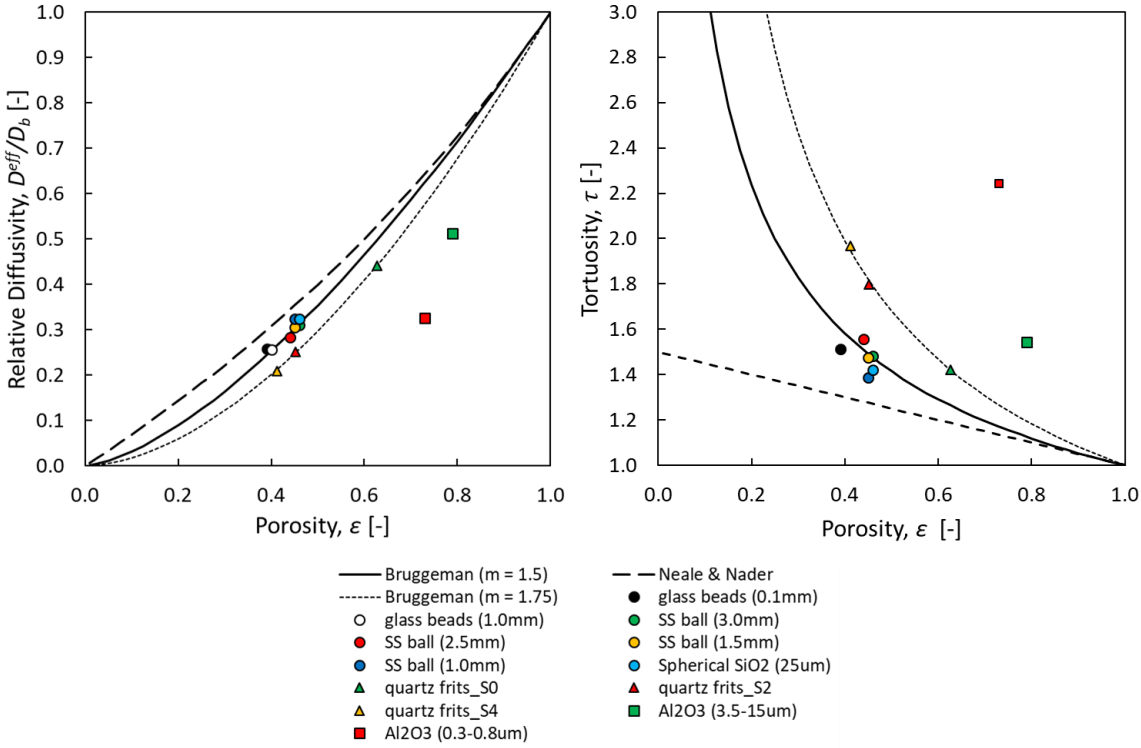

Figure 6 Relative diffusivity (left) and tortuosity (right) of porous media and comparison to the theoretical correlations. (Each data point is an average of three measurements. Error bar omitted for clarity)

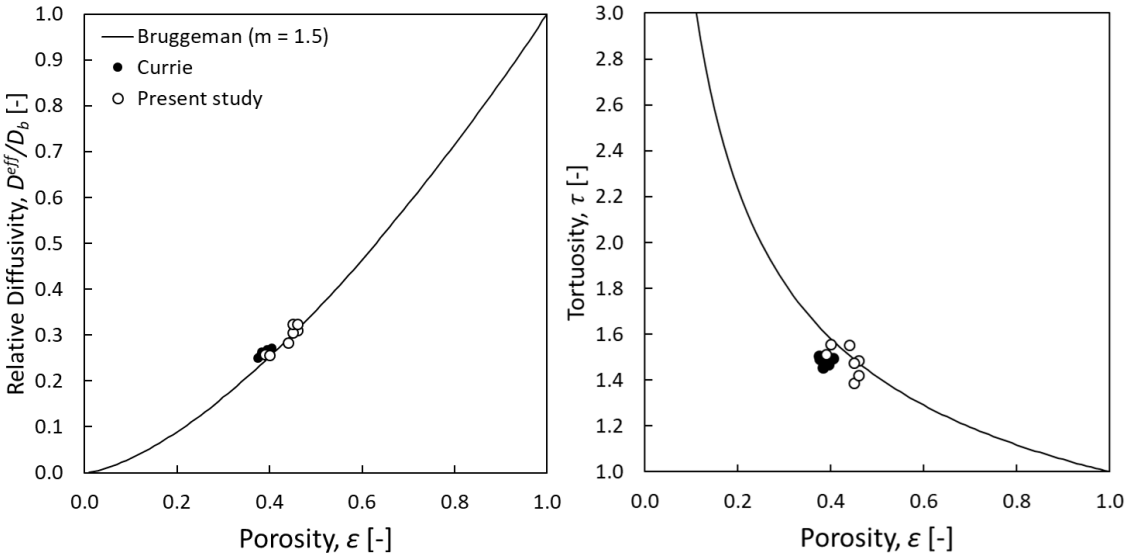

Figure 7 Comparison of the relative diffusivity (left) and the tortuosity (right) between Currie [35] and the present study (m = 1.5)

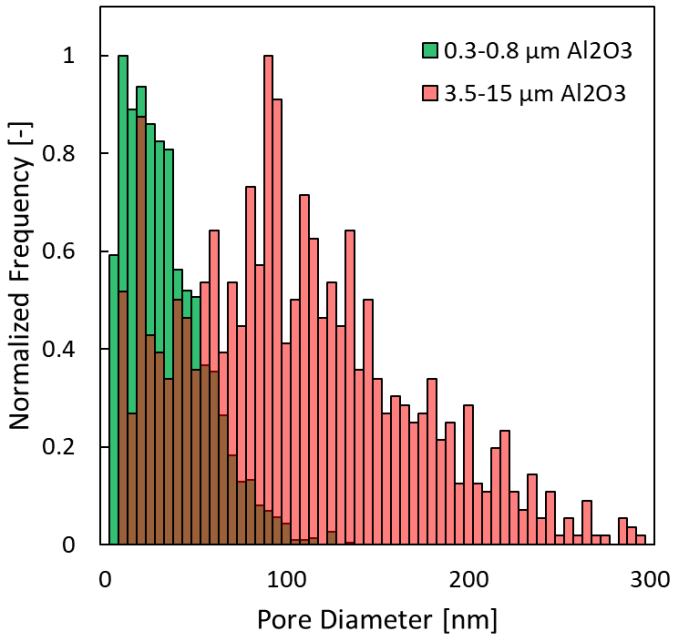

Figure 8 Pore size distributions of 0.3-0.8 µm Al_2O_3 packing (green) and 3.5-15 µm Al_2O_3 packing (red)